Secondary Flows of Simplified Phan-Thien Tanner (SPTT) Non-Linear Viscoelastic Fluid Between Parallel Rotating Disks

Seyed Hassan Hashemabadi, Seyed Mohammad Mirnajafizadeh*

Summary: The steady state laminar flow of non-linear viscoelastic fluid with Simplified Phan-Thien Tanner (SPTT) model between coaxial rotating disks is studied analytically. With linearized stress coefficient in the constitutive equation (SPTT), primary flow and weak secondary flow have been investigated by perturbation techniques while the aspect ratio is very small. Axial and radial velocity profiles arising from secondary flow are completely analyzed for various boundary conditions and properties of the viscoelastic fluid. The results indicate the strong effects of the elasticity and boundary conditions on velocity profiles. The inertial secondary flow consists of a single vortex for co-rotating disks and two vortices for counter-rotating disks which is well represented by the approximate analytical solution.

Keywords: analytical solution; coaxial rotating disks; secondary flow; SPTT model; viscoelastic fluid

Introduction

The torsional motions of a fluid between a rotating cone and plate and between two rotating coaxial parallel disks are used extensively in rheometry to measure the material properties that characterize non-Newtonian fluids. Von Karman introduced an ingenious similarity transformation to study the axisymmetric flow induced by a single rotating disk. Bhatnagar[1] showed that this transformation can be used even when the fluid is confined between two parallel disks rotating about a common axis at different speeds. These two works have been followed by extensive studies on the swirling flow for linear viscous fluids.

Phan-Thien[2] demonstrates that the solution of the unsteady state flow between rotating disks for a Maxwell fluid could be reduced to solving a system of coupled ordinary differential equations, consisting of the equations of motion and the constitutive relations. Following upon this work Phan-Thien[3] showed that the same situation arises with the Oldroyd-B fluid, which includes the Newtonian and the Maxwell fluid as special cases. He has also discussed the linearized stability of the torsional flow, which is the steady shearing motion, between the two plates and found that the flow is unstable at high values of the Weissenberg number. Ji et al. have carried out a detail investigation of the flow an Oldroyd-B fluid using an analytic continuation method that exhibit turning points and bifurcation points and their solution includes the results of Maxwell model as a special case.[4] Another analysis was carried out by Crewther et al. wherein they study steady and unsteady axisymmetric flows of an Oldroyd-B fluid between rotating plates.[5] Their results on steady flows covered the results of Ji. et al.'s work. Rajagopal reviewed the efforts that have been expended in the study of both symmetric and asymmetric solutions in

Computational Fluid Dynamics Research Laboratory, Department of Chemical Engineering, Iran University of Science and Technology, Narmak, Tehran, 16846, Iran
Fax: (+98) 21 7724-0495;
E-mail: hashemabadi@iust.ac.ir

the case of both the classical linearly viscous fluid and viscoelastic fluids (Second order model, Maxwell model, and Oldroyd-B model).[6]

The Oldroyd-B constitutive equation predicts a constant viscosity and a constant first normal stress coefficient, and thus it is relatively a simple model for viscoelastic flows. The model is very suitable for Boger fluids that have nearly constant viscosities up to high shear rates. The Phan-Thien–Tanner (PTT) model is a fairly simple quasi-linear viscoelastic model constitutive equation, which was derived using network theory by Phan-Thien and Tanner[7] and Phan-Thien[8]. This model incorporates not only shear viscosity and normal-stress differences but also an elongational parameter ε and so reproduces many of the characteristics of the rheology of polymer solutions and other non-Newtonian liquids. The PTT model has attracted author's attention and considerable papers have been published by using this model. Oliveira et al. used Simplified PTT constitutive equation to obtain an analytical solution for fully-developed pipe and channel flows.[9] Alves et al. studied the steady pipe and channel flows of a single mode Phan-Thien-Tanner.[10] Axial annular flow of nonlinear viscoelastic PTT fluid was modeled analytically by Pinho and Oliveira.[11] Hashemabadi et al. provided a series of solutions for Couette-Poiseuille flow of SPTT fluid between parallel plates.[12] Skewed Poisueille-Couette flows of SPTT fluids in concentric annuli and channels were investigated by Cruz and Pinho.[13] Mirzazadeh et al. solved analytically purely tangential flow of PTT viscoelastic flow in a concentric annulus with relative rotation of the inner and outer cylinders.[14] Extensive investigations in relation to heat transfer and effective parameters for PTT constitutive equation have been presented in the literatures in recent years.[15–19]

The solution of secondary flows of Phan-Thien-Tanner (PTT) model fluid moving between rotational coaxial disks has not yet been reported. The objective of the present investigation is to solve analytically the momentum equations for simplified PTT fluid, the primary and weak secondary flows are derived where the upper and lower disks are rotating with different angular velocities, for a wide range of Deborah numbers.

Governing Equations

Figure 1 shows two coaxial disks of radius a with distance h where $a \gg h$. The top and bottom plates rotate with constant angular speed Ω and $s\Omega$ respectively. The flow is assumed to be laminar, steady state, isothermal, axis-symmetric and incompressible. The no slip and no penetration condition exist at the walls and gravitational forces for the flow domain are negligible. In the following discussion a cylindrical coordinate system (r', θ', z') will be used. The continuity and motion equations are[20]:

$$\nabla \cdot \mathbf{v} = 0 \tag{1}$$

$$\mathbf{v} \cdot \nabla \mathbf{v} = -\nabla p' + \nabla \cdot \boldsymbol{\tau} \tag{2}$$

The extra stresses are given here by the simplified form of the Phan-Thien Tanner (PTT) constitutive equation:

$$Z(tr\boldsymbol{\tau})\boldsymbol{\tau} + \lambda \hat{\boldsymbol{\tau}} = 2\eta \mathbf{D} \tag{3}$$

Where D is deformation rate tensor, λ is the relaxation time, η is the viscosity coefficient and ε is a parameter of the model limiting the extensional viscosity of the fluid. The pre-stress function $Z(tr\tau)$ is the linearization form of the more general

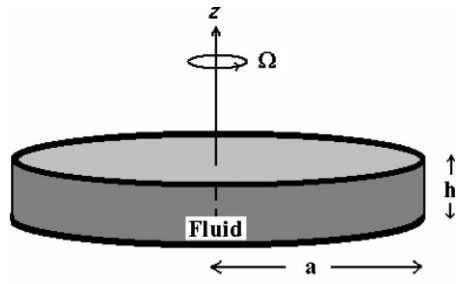

Figure 1.
Schematic diagram of coaxial disks.

exponential coefficient that can be written as follow:

$$Z(tr\boldsymbol{\tau}) = 1 + \frac{\varepsilon\lambda}{\eta} tr\boldsymbol{\tau}$$

Oldroyd's upper convective derivative $\hat{\boldsymbol{\tau}}$ is defined as:

$$\hat{\boldsymbol{\tau}} = \frac{D\boldsymbol{\tau}}{Dt'} - \boldsymbol{\tau}.\nabla\mathbf{v} - (\nabla\mathbf{v})^{\dagger}\cdot\boldsymbol{\tau} \tag{4}$$

Where velocity gradient tensor$\nabla\mathbf{v}$, for the problem depicted above, is simplified as:

$$\nabla\mathbf{v} = \begin{pmatrix} \frac{\partial v_r}{\partial r} & 0 & \frac{\partial v_z}{\partial r} \\ -\frac{v_\theta}{r} & \frac{v_r}{r} & 0 \\ \frac{\partial v_r}{\partial z} & \frac{\partial v_\theta}{\partial z} & \frac{\partial v_z}{\partial z} \end{pmatrix}$$

And $\nabla\mathbf{v}^{\dagger}$ is transpose of velocity gradient tensor.

It is convenient to introduce following dimensionless variables[5]:

$$r = r'/a; \quad z = z'/h$$

$$u = v_r/a\Omega; \quad v = v_\theta/a\Omega; \quad w = v_z/h\Omega;$$
$$p = \alpha^2(p'/\eta\Omega)$$

$$\Sigma = \alpha^2\tau_{rr}/\eta\Omega; \quad \zeta = \alpha^2\tau_{r\theta}/\eta\Omega;$$
$$\Upsilon = (\alpha\tau_{rz}/\eta\Omega)$$

$$\Delta = \left(\alpha^2\tau_{\theta\theta}/\eta\Omega\right); \quad \Pi = (\alpha\tau_{\theta z}/\eta\Omega);$$
$$\Gamma = \tau_{zz}/(\eta\Omega)$$

$$\mathrm{Re} = \rho\Omega a^2/\eta; \quad De = \lambda\Omega$$

Where α is the aspect ratio and represents the ratio of distance between two parallel disks to radius *h/a*. For steady axis-symmetric flow, the dimensionless equations of continuity and motion are respectively:

$$\frac{\partial u}{\partial r} + \frac{u}{r} + \frac{\partial w}{\partial z} = 0 \tag{5}$$

$$\alpha^2\mathrm{Re}\left(u\frac{\partial u}{\partial r} + w\frac{\partial u}{\partial z} - \frac{v^2}{r}\right) = -\frac{\partial p}{\partial r} + \frac{\partial\Sigma}{\partial r} + \frac{\partial\Upsilon}{\partial z} + \frac{1}{r}(\Sigma - \Delta) \tag{6}$$

$$\alpha^2\mathrm{Re}\left(u\frac{\partial v}{\partial r} + w\frac{\partial v}{\partial z} + \frac{uv}{r}\right) = \frac{\partial\zeta}{\partial r} + \frac{2}{r}\zeta + \frac{\partial\Pi}{\partial z} \tag{7}$$

$$\frac{\partial p}{\partial z} = \alpha^2\left[\frac{\partial\Gamma}{\partial z} + \frac{\partial\Upsilon}{\partial r} + \frac{\Upsilon}{r}\right] \tag{8}$$

From tensor analysis of SPTT fluid model as a constitutive equation can be obtained:

$$Z(tr\boldsymbol{\tau})\Sigma = -De\left[u\frac{\partial\Sigma}{\partial r} + w\frac{\partial\Sigma}{\partial z} - 2\Sigma\frac{\partial u}{\partial r} - 2\Upsilon\frac{\partial u}{\partial z}\right] + 2\alpha^2\frac{\partial u}{\partial r} \tag{9}$$

$$Z(tr\boldsymbol{\tau})\zeta = -De\left\{\begin{matrix} u\frac{\partial\zeta}{\partial r} + w\frac{\partial\zeta}{\partial z} + \Sigma\left(\frac{v}{r} - \frac{\partial v}{\partial r}\right) \\ -\zeta\left(\frac{u}{r} + \frac{\partial u}{\partial r}\right) - \Upsilon\frac{\partial v}{\partial z} - \Pi\frac{\partial u}{\partial z} \end{matrix}\right\} + \alpha^2\left(\frac{\partial v}{\partial r} - \frac{v}{r}\right) \tag{10}$$

$$Z(tr\boldsymbol{\tau})\Upsilon = -De\left\{\begin{matrix} u\frac{\partial\Upsilon}{\partial r} + w\frac{\partial\Upsilon}{\partial z} - \Sigma\frac{\partial w}{\partial r} \\ -\Upsilon\left(\frac{\partial w}{\partial z} + \frac{\partial u}{\partial r}\right) - \Gamma\frac{\partial u}{\partial z} \end{matrix}\right\} + \frac{\partial u}{\partial z} + \alpha^2\frac{\partial w}{\partial r} \tag{11}$$

$$Z(tr\boldsymbol{\tau})\Delta = -De\left\{\begin{matrix} u\frac{\partial\Delta}{\partial r} + w\frac{\partial\Delta}{\partial z} - 2\Delta\frac{u}{r} \\ +2\zeta\left(\frac{v}{r} - \frac{\partial v}{\partial r}\right) - 2\Pi\frac{\partial v}{\partial z} \end{matrix}\right\} + 2\alpha^2\frac{u}{r} \tag{12}$$

$$Z(tr\boldsymbol{\tau})\Pi = -De\left\{\begin{matrix} u\frac{\partial\Pi}{\partial r} + w\frac{\partial\Pi}{\partial z} + \Upsilon\left(\frac{v}{r} - \frac{\partial v}{\partial r}\right) \\ -\Pi\left(\frac{u}{r} + \frac{\partial w}{\partial z}\right) - \xi\frac{\partial w}{\partial r} - \Gamma\frac{\partial v}{\partial z} \end{matrix}\right\} + \frac{\partial v}{\partial z} \tag{13}$$

$$Z(tr\boldsymbol{\tau})\Gamma = -De\left\{\begin{matrix} u\dfrac{\partial}{\partial r}\Gamma + w\dfrac{\partial}{\partial z}\Gamma - 2\Upsilon\dfrac{\partial w}{\partial r} \\ -2\Gamma\dfrac{\partial w}{\partial z}\end{matrix}\right\} + 2\frac{\partial w}{\partial z} \quad (14)$$

Where

$$Z(tr\boldsymbol{\tau}) = \left[1 + \frac{\varepsilon De}{\alpha^2}\left(\Sigma + \Delta + \alpha^2\Gamma\right)\right]$$

The normalized boundary conditions are

At $z = 0 \quad u = w = 0,\ v = sr$ (15)

At $z = 1 \quad u = w = 0,\ v = r$ (16)

At $r = 0 \quad u = v = \frac{\partial w}{\partial r} = 0$ (17)

Where s is coefficient of angular velocity.

Linearizing the Equations

Consider dependent variables in the following general form:

$$q = q_0 + q_2$$

Where subscripts 0 and 2 represent primary and secondary flows respectively. So we have:

$$q \equiv \{u, v, w, p, \Sigma, \zeta, \Upsilon, \Pi, \Gamma\}$$

q_0 shows the primary flow variables and q_2 is assumed to be small perturbations that achieve a significant importance for analysis of secondary flows. By considering just the primary flow and assuming that the aspect ratio is very small, the governing equations are simplified. This case is satisfied while the type of flow is steady creeping flow in which just the dimensionless θ-component of velocity exists and the radial and axial components of velocity are zero:

$$u_0 = w_0 = 0, \quad v_0 = v_0(r, z), \quad p_0 = p_0(r) \quad (18)$$

By considering the conditions depicted in Eq. (18) and assuming the aspect ratio α, is very small, the momentum and constitutive equations are simplified respectively:

$$\frac{\partial \Pi_0}{\partial z} = 0 \quad (19)$$

$$\frac{dp_0}{dr} = -\frac{\Delta_0}{r} \quad (20)$$

$$\boldsymbol{\tau}_0 = \begin{pmatrix} 0 & 0 & 0 \\ 0 & \Delta_0 & \Pi_0 \\ 0 & \Pi_0 & 0 \end{pmatrix} \quad (21)$$

$$[1 + \varepsilon De\Delta_0]\Pi_0 = \frac{\partial v_0}{\partial z} \quad (22)$$

$$[1 + \varepsilon De\Delta_0]^2\Delta_0 = 2De\left(\frac{\partial v_0}{\partial z}\right)^2 \quad (23)$$

Substituting Eq. (22) into Eq. (19) leads to a differential equation for velocity v_0, that can be solve with the following boundary conditions:

At $z = 0 \quad v_0 = sr$

At $z = 1 \quad v_0 = r$

Finally, the velocity profile is calculated:

$$v_0 = r[(1 - s)z + s] \quad (24)$$

Using the velocity profile Eq. (24), into Eq. (23), and solving the cubic equation forΔ_0 leads to one real root:

$$\Delta_0 = \frac{\left(\frac{1+27\varepsilon De^2r^2(1-s)^2+3\sqrt{3}\varepsilon De r(1-s)}{\sqrt{2+27\varepsilon De^2r^2(1-s)^2}}\right)^{1/3}}{\varepsilon De} + \frac{1}{\left(\frac{1+27\varepsilon De^2r^2(1-s)^2+3\sqrt{3}\varepsilon De r(1-s)}{\sqrt{2+27\varepsilon De^2r^2(1-s)^2}}\right)^{1/3}} - \frac{2}{3\varepsilon De} \quad (25)$$

Weak Secondary Flows

The secondary flow is obtained when the perturbation is taken into account. Also the solution goes on with respect to the solution of primary flow. For this reason, we try to keep the terms in equations that combination of them makes a remarkable amount, with this approach, continuity and momentum equations, Eq. (5)–(14), are changed as follows:

$$\frac{\partial u_2}{\partial r} + \frac{u_2}{r} + \frac{\partial w_2}{\partial z} = 0 \quad (26)$$

$$\frac{\partial p_2}{\partial r} = \mathrm{Re}\frac{v_0^2}{r} + \frac{\partial \Upsilon_2}{\partial z} - \frac{1}{r}\Delta_2 \quad (27)$$

$$\frac{\partial \zeta_2}{\partial r}+\frac{2}{r}\zeta_2+\frac{\partial \Pi_2}{\partial z}=0 \tag{28}$$

$$\frac{\partial p_2}{\partial z}=0 \tag{29}$$

Stress tensor components equations are simplified to:

$$\Sigma_2=0 \tag{30}$$

$$(1+\varepsilon De\Delta_0)^2\zeta_2=2De\frac{\partial v_0}{\partial z}\frac{\partial u_2}{\partial z} \tag{31}$$

$$(1+\varepsilon De\Delta_0)\Upsilon_2=\frac{\partial u_2}{\partial z} \tag{32}$$

$$(1+\varepsilon De\Delta_0)^2\Delta_2 = 2De\begin{pmatrix}\frac{3De}{(1+\varepsilon De\Delta_0)}\left(\frac{\partial v_0}{\partial z}\right)^2\frac{\partial w_2}{\partial z}\\ +2\frac{\partial v_0}{\partial z}\frac{\partial v_2}{\partial z}\end{pmatrix} \tag{33}$$

$$(1+\varepsilon De\Delta_0)\Pi_2 = \frac{3De}{(1+\varepsilon De\Delta_0)}\frac{\partial v_0}{\partial z}\frac{\partial w_2}{\partial z}+\frac{\partial v_2}{\partial z} \tag{34}$$

$$(1+\varepsilon De\Delta_0)\Gamma_2=2\frac{\partial w_2}{\partial z} \tag{35}$$

The boundary conditions suggest that a solution can be found of the following form[20]:

$$v=rG(z) \tag{36}$$

If we let u and w depend on $z$through a second function$H(z)$then the continuity equation requires that:

$$u=r\frac{dH(z)}{dz},\quad w=-2H(z) \tag{37}$$

Also, the following functions are suggested for dimensionless stress components[5]:

$$\begin{aligned}&\Sigma=r^2\tilde{\Sigma}(z),\quad \zeta=r^2\tilde{\zeta}(z),\quad \Upsilon=r\tilde{\Upsilon}(z)\\ &\Delta=r^2\tilde{\Delta}(z),\quad \Pi=r\tilde{\Pi}(z),\\ &\Gamma=\tilde{\Gamma}(z)\end{aligned} \tag{38}$$

The stress components with hat can be derived from Eq. (31)–(35) directly. After differentiation of Eq. (27) with respect to z and using the compatibility condition, $\frac{\partial^2 p_2}{\partial r\partial z}=0$ resulted from Eq. (29) and substitution of hat stress components can be concluded:

$$\frac{2De(1-s)}{(1+\varepsilon De\Delta_0)^2}\begin{pmatrix}2\frac{\partial^2 G(z)}{\partial z^2}-\frac{6De}{(1+\varepsilon De\Delta_0)}\\ (1-s)\frac{\partial^2 H(z)}{\partial z^2}\end{pmatrix} -\frac{1}{(1+\varepsilon De\Delta_0)}\frac{\partial^4 H(z)}{\partial z^4}=2\mathrm{Re}v_0\frac{\partial v_0}{\partial z} \tag{39}$$

From substituting of stress components with hat into Eq. (28) and simplifying it gives:

$$\frac{\partial^2 G(z)}{\partial z^2}+\frac{2De(1-s)}{1+\varepsilon De\Delta_0}\frac{\partial^2 H(z)}{\partial z^2}=0 \tag{40}$$

Combination of Eq. (39) and Eq. (40) and after rearrangement can be obtained:

$$\frac{\partial^4 H(z)}{\partial z^4}+\Lambda^2\frac{\partial^2 H(z)}{\partial z^2}=Az+B \tag{41}$$

Where

$$\begin{aligned}&\Lambda^2=\frac{20De^2(1-s)^2}{(1+\varepsilon De\Delta_0)^2}\\ &A=-2\mathrm{Re}(1+\varepsilon De\Delta_0)(1-s)^2,\\ &B=-2\mathrm{Re}\,s(1-s)(1+\varepsilon De\Delta_0)\end{aligned} \tag{42}$$

From solution of Eq. (41), H(z) can be calculated as follow:

$$H(z)=\frac{1}{\Lambda^2}\left[\frac{1}{2}z^2\left(\frac{1}{3}Az+B\right)-(C_1\cos(\Lambda z)+C_2\sin(\Lambda z))\right]+C_3z+C_4 \tag{43}$$

We now have four integration constants to determine by using these four additional boundary conditions:

$$\begin{aligned}&H(0)=0,\quad H(1)=0\\ &H'(0)=0,\quad H'(1)=0\end{aligned} \tag{44}$$

Constants of Eq. (43) can be found as follows:

$$\begin{aligned}&C_1=\tfrac{1}{6}\left\{\tfrac{\Lambda\cos\Lambda(A+3B)-3\sin\Lambda(A+2B)+\Lambda(2A+3B)}{\Lambda(\Lambda\sin\Lambda-2+2\cos\Lambda)}\right\}\\ &C_2=\tfrac{1}{6}\left\{\tfrac{3\sin\Lambda(A+2B)-\Lambda(A+3B)(1+\cos\Lambda)}{\Lambda(2\sin\Lambda-\Lambda\cos\Lambda-\Lambda)}\right\}\\ &C_3=\tfrac{1}{\Lambda}C_2,\quad C_4=\tfrac{1}{\Lambda^2}C_1\end{aligned}$$

From insertion of Eq. (43) into Eq. (40) and integration and using of boundary

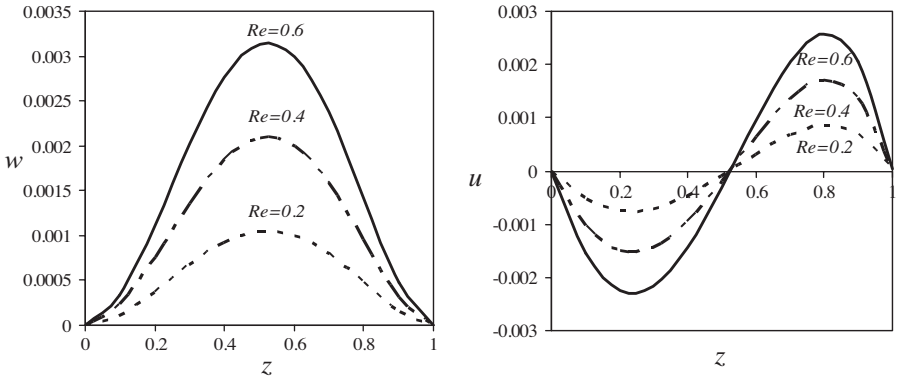

Figure 2.
Axial and radial velocity profile when s = 0, De = 0 (Newtonian Fluid).

conditions Eq. (15) and (16), G(z) can be derived as follow:

$$G(z) = -\frac{2De(1-s)}{\Lambda^2(1+\varepsilon De\Delta_0)} \left[\frac{1}{2}z^2\left(\frac{1}{3}Az + B\right) - (C_1\cos(\Lambda z) + C_2\sin(\Lambda z))\right] + C_5 z + C_6 \quad (45)$$

Where

$$C_5 = s + C_1\frac{2De(1-s)}{\Lambda^2(1+\varepsilon De\Delta_0)}$$

$$C_6 = 1 - s + \frac{2De(1-s)}{\Lambda^2(1+\varepsilon De\Delta_0)} \left[\frac{1}{6}A + \frac{1}{2}B - C_1(\cos(\Lambda)+1) - C_2\sin(\Lambda)\right]$$

Now three components of velocity v, u, w can be calculated with two function of H(z) and G(z) according to Eq. (36) and (37).

Results and Discussion

Effects of Reynolds number, elongational parameter and Deborah number as well as boundary conditions on the flow field were investigated and finally velocity vectors were depicted for two different boundary conditions. In Figure 2 (it was considered the lower plate is at the rest s = 0) and Figure 3 (when the lower disk rotates five times faster than upper one s = 5) for Newtonian fluid (De = 0) illustrate the corresponding axial and radial velocities

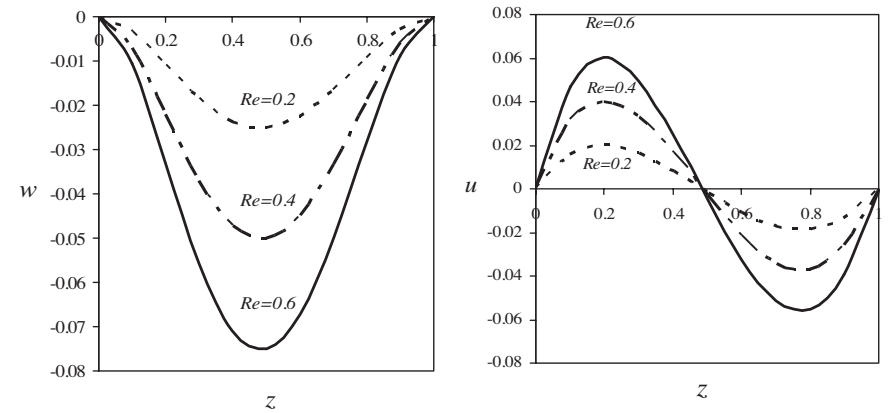

Figure 3.
Axial and radial velocity profile when s = 5, De = 0 (Newtonian Fluid).

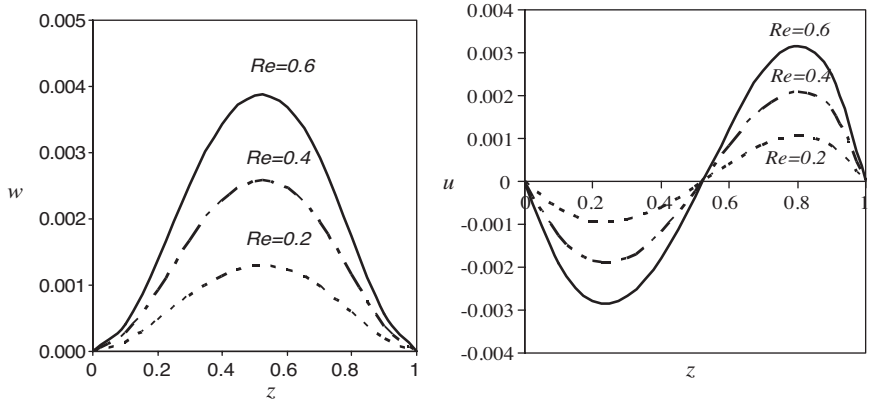

Figure 4.
Axial and radial velocity profile when $s = 0$, $De = 0.5$ and $\varepsilon = 1$.

between two parallel disks. The results show good agreement with previous work.[7] In Figure 4, it was considered the lower plate is at the rest and the fluid is a viscoelastic fluid which $De = 0.5$ and $\varepsilon = 1$. As it is obvious, with viscoelasticity effects haven't changed the trend of secondary flow between coaxial disks relative to Newtonian fluid, but these properties can strengthen or weaken the axial and radial flows in the fluid. Axial velocity profile for this flow conditions is nearly parabolic and is positive everywhere. On the other hand, radial velocity is negative in the lower half region whereas it is positive in the upper half region between the two parallel disks. With promotion of Reynolds number increases maximum of absolute u-velocity in two regions. Comparison of viscoelastic and Newtonian fluids behavior while the lower disk is at the rest, at $Re = 0.4$, shows the maximum of axial velocity has almost 19% growth. Figure 5 shows while the lower disk rotates five times faster than upper one, same as the Newtonian fluid, the axial velocity becomes completely negative and the profile is nearly parabolic, but the maximum has changed considerably (300% growth). For radial velocity profile due to inertia effects, the values is positive in the lower half region whereas it is negative in the upper half region between the two disks. Comparing these curves with the corresponding curves for $s = 0$ in Figure 2

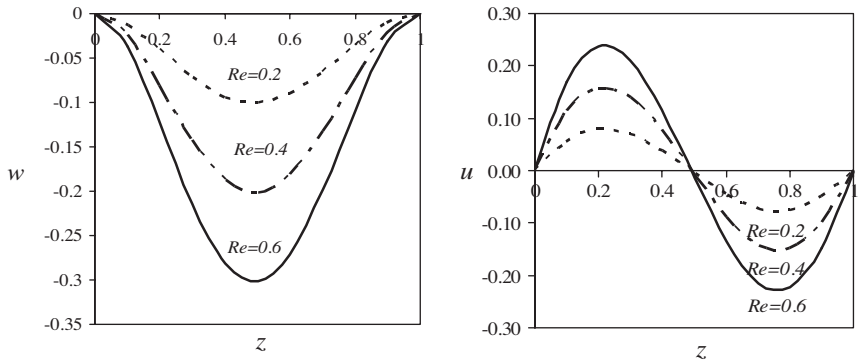

Figure 5.
Axial and radial velocity profile when $s = 5$, $De = 0.5$ and $\varepsilon = 1$.

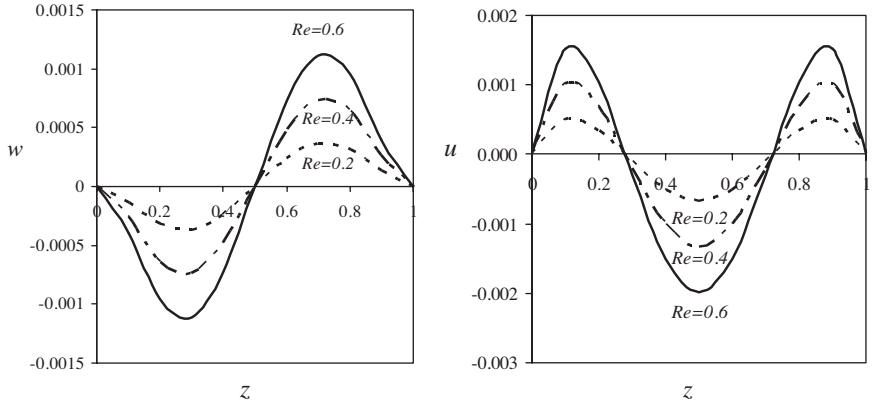

Figure 6.
Axial and radial velocity profile when $s = -1$, $De = 0.5$ and $\varepsilon = 1$.

we found that the flow field has been reversed. When the two disks rotate with same angular velocity but in opposite direction $s = -1$, Figure 6 illustrates the distribution of w-velocity for $Re = 0.2$, 0.4 and 0.6. Axial velocity is positive but only in the upper half region and in the lower half region, it takes negative values. For radial velocity, the flow region for the related boundary condition is divided into three parts with the appearance of a central core in which dimensionless u-velocity is negative for all values of Re. In the other two regions, one near the lower disk and the other near the upper disk, u-velocity is positive. Figure 7 shows effect of elongational parameter on axial and radial velocity profiles. As it can be seen, the decrease of elongation effects promotes the magnitude of dimensionless axial and radial velocities. This is not valid for variation of Deborah number, as it is clear from Figure 8, increasing of Deborah number which gives the relative importance of elasticity in the fluid, improves the magnitude of secondary flows between parallel disks. Therefore elongational parameter (ε) and Deborah number (De) have opposite effects, but the Deborah number has more noticeable influence on secondary flows between two disks. Figure 9 illustrates the vector plot of secondary flows while the

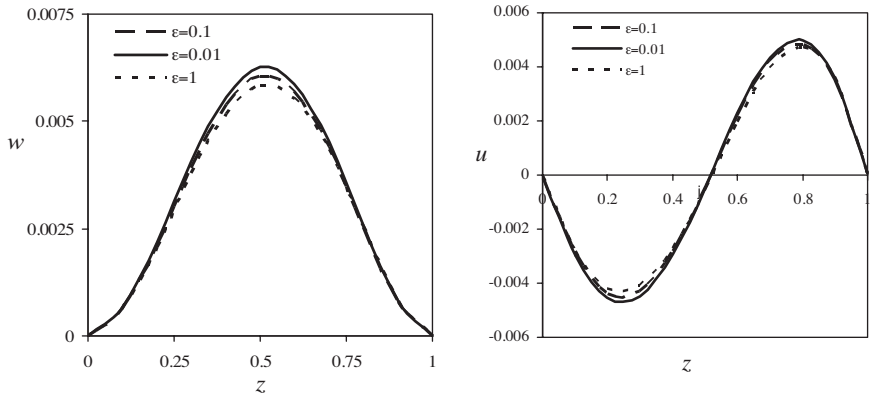

Figure 7.
Effect of elongation parameter on axial and radial velocity profile ($Re = 0.6$, $s = 0$ and $De = 1$).

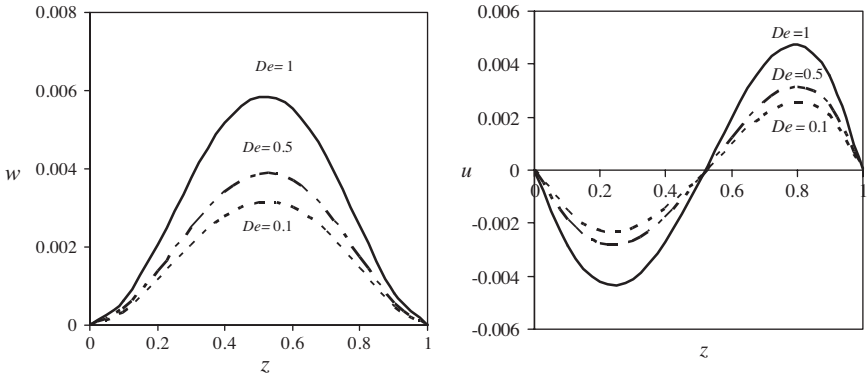

Figure 8.
Effect of Deborah number on axial and radial velocity profile ($\varepsilon = 1$, s = 0 and Re = 0.6).

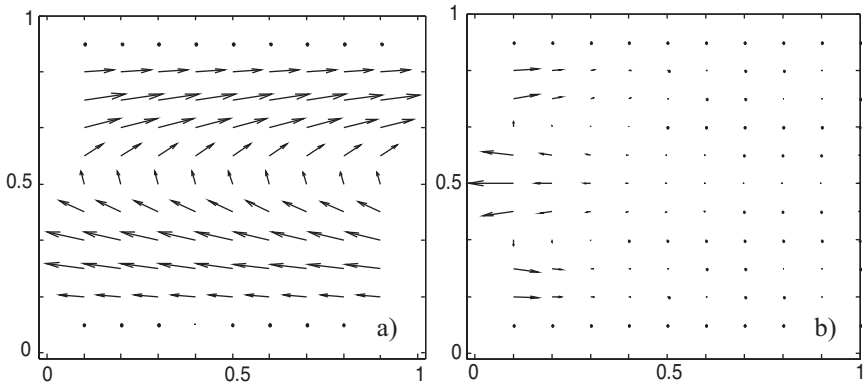

Figure 9.
Velocity vectors between two parallel rotating disks for De = 1, Re = 0.6 and a) s = 0, b) s = −1

lower disk is at the rest (s = 0) and two disks rotate reverse (s = −1) respectively. As it's shown, there is only one vortex for co-rotating plates ($s \geq 0$)and two vortices for counter rotating disks ($s < 0$). As s decreases from zero, one small vortex near the lower plate appears and with more decreasing of s, this vortex becomes bigger and can be found two equal vortices between parallel disks while two disks rotate opposite each other with same angular velocity ($s = -1$).

Conclusion

The steady axisymmetric laminar flow of simplified Phan-Thien–Tanner (SPTT) model fluid between coaxial rotating disks has been investigated analytically. Weak secondary flows were analyzed by the perturbation technique when the aspect ratio is very small. Radial and axial velocities for various conditions were illustrated. When the lower disk is stationary and upper disk rotates with a constant angular velocity, axial velocity is positive and nearly parabolic. Radial velocity is divided to two regions, negative in the lower half and positive in the upper half region. When both disks rotate with the same velocity but in opposite direction, axial velocity is positive and negative in upper and lower half regions respectively. Radial velocity for this situation consisted up three parts, negative at the centre and

positive both in the upper and lower regions. Deborah number and elongational parameter affect the values of secondary flows. Deborah number increases the values of axial and radial velocities while elongational parameter decreases. A usual phenomenon in flow of rotating disk is existence of vortex between the disks. For co-rotating disks, there is only one vortex and two vortices for counter rotating disks.

[1] R. K. Bhatnagar, *Int. J. Math. & Math. Sci.* **1981**, *4*, 181.
[2] N. Phan-Thien, *J. Fluid Mechanics* **1983**, *128*, 427.
[3] N. Phan-Thien, *J. Non-Newtonian Fluid Mechanics* **1983**, *13*, 325.
[4] Z. H. Ji, K. R. Rajagopal, A. Z. Szeri, *J. Non-Newtonian Fluid Mechanic* **1990**, *36*, 1.
[5] I. Crewther, R. R. Huilgol, R. Jozsa, *Physical Sciences and Engineering* **1991**, *337*(1648), 467.
[6] K. R. Rajagopal, *Theoretical and Computational Fluid Dynamics* **1992**, *3*, 185.
[7] N. Phan-Thien, R. I. Tanner, *J. Non-Newtonian Fluid Mechanic* **1977**, *2*, 353.
[8] N. Phan-Thien, *J. Rheology* **1978**, *22*, 259.
[9] P. J. Oliviera, F. T. Pinho, *J. Fluid Mechanics* **1999**, *387*, 271.
[10] M. A. Alves, F. T. Pinho, P. J. Oliviera, *J. Non-Newtonian Fluid Mechanic* **2001**, *101*, 55.
[11] F. T. Pinho, P. J. Oliveira, *J. Non-Newtonian Fluid Mechanic* **2000**, *93*, 325.
[12] S. H. Hashemabadi, S. Gh. Etemad, J. Thibault, M. R. Golkar Naranji, *Int. J. of Heat and Fluid Flow* **2003**, *24*, 137.
[13] D. O. A. Cruz, F. T. Pinho, *J. Non-Newtonian Fluid Mechanic* **2004**, *121*, 1.
[14] M. Mirzazadeh, M. P. Escudier, F. Rashidi, S. H. Hashemabadi, *J. Non-Newtonian Fluid Mechanic* **2005**, *129*, 88.
[15] F. T. Pinho, P. J. Olivieira, *Int. J. Heat and Mass Transfer* **2000**, *43*, 2273.
[16] P. M. Coelho, F. T. Pinho, P. J. Olivieira, *Int. J. Heat and Mass Transfer* **2002**, *45*, 1413.
[17] P. M. Coelho, F. T. Pinho, P. J. Olivieira, *Int. J. Heat and Mass Transfer* **2003**, *46*, 3865.
[18] S. H. Hashemabadi, S. Gh. Etemad, J. Thibault, *Int. J. Heat and Mass Transfer* **2004**, *47*, 3985.
[19] P. M. Coelho, F. T. Pinho, *Int. J. Heat and Mass Transfer* **2006**, *20*, 3349.
[20] R. B. Bird, R. C. Armstrong, O. Hassager, *Dynamics of Polymeric Liquids*, 2nd ed., vol. 1, Jon Wiley, **1987**.

